Research on Engineering Structures & Materials
www.jresm.org
Research Group

Research Article

Computational fluid dynamics analysis of wind loading on antennas attached to a telecommunication tower

Patrick Kazadi [*,a], Chris Ackerman [b], Andrei Kolesnikov [c]

Department of Civil Engineering, Faculty of Engineering and the Built Environment, Tshwane University of Technology, Pretoria, South Africa

Article Info

Article History:

Received 22 Dec 2025

Accepted 19 May 2026

Keywords:

Computational fluid dynamics;
Antenna;
Monopole mast;
Wind loading;
Force coefficients;
Dynamic pressure

Abstract

The rapid expansion of telecommunication infrastructure has increased the need for reliable structural assessments of monopole towers as antennas are added or reconfigured. Traditionally, these assessments assume independent wind loading exposure for each antenna using conservative force coefficients or making use of wind tunnel often leading to overdesign. This study investigates the application of Computational Fluid Dynamics (CFD) as a more accurate and cost-efficient alternative. Using ANSYS Fluent and CATIA V5, a variety of antenna configurations were modeled and analyzed under steady-state wind conditions. The results demonstrated that bending moments predicted for clustered antenna arrangements were up to 52% lower than those obtained from traditional design standard codes such as TIA-222 and SANS 10225. These reductions are primarily due to aerodynamic shielding effects. The study highlights CFD as a reliable design tool for telecommunication towers, validated against wind tunnel data and supported by mesh independence studies conducted. These findings suggest that CFD offers a more accurate and cost-efficient alternative to traditional conservative assumptions, with the potential to optimize structural design and reduce material usage. It confirms the potential of CFD, using a standard laptop to reduce conservatism in structural design, and time without compromising safety.

© 2026 MIM Research Group. All rights reserved.

1. Introduction

Telecommunication towers are critical infrastructure enabling mobile and wireless communication. These towers, which include monopoles, lattice structures, guyed masts, and camouflaged artificial trees, are designed to elevate antennas for optimal signal transmission to certain heights. As the telecommunications sector evolves rapidly, frequent updates to antenna configurations necessitate accurate structural assessments to ensure tower integrity.

Traditionally, registered professionals rely on the use of wind tunnel testing or conservative design standard codes to evaluate wind loading on towers. However, wind tunnel facilities such as those operated by the Council for Scientific and Industrial Research (CSIR) are not always accessible, and code-based methods may result in overdesign due to simplifications and conservative assumptions.

This study aims to:

- Evaluate the use of CFD to simulate wind effects on telecommunication towers with various antenna configurations, scale geometry modelled from CATIA V5.
- Compare CFD results against wind tunnel data and established standards design code.

*Corresponding author: patmutombo7@gmail.com
[a]orcid.org/0009-0000-4485-5631; [b]orcid.org/0009-0007-3162-3496; [c]orcid.org/0000-0001-9095-8666
DOI: http://dx.doi.org/10.17515/resm2026-1427st1222rs

- Determine the reduction in bending moment and conservatism achievable through CFD results analysis.
- Demonstrate the practicality and efficiency of conducting such analyses on standard computing hardware.
- Assess the feasibility to extract and process specific force coefficient of antenna configurations, at different heights for design purposes.

While traditional methods such as wind tunnel testing and standard design codes remain invaluable. In this study, CFD has proven its ability, with a positive outcome that was successfully compared with the existing data. Additionally, CFD gives registered professionals more options to generate useful data if needed for telecommunications infrastructure design and analysis.

2. Methodology

Scaled 3D geometries of monopole towers with different antenna arrangements were created using CATIA V5, as shown in (Fig. 1). Five configurations were analyzed: a bare mast, and mast with one, two, three, and six antennas arranged in radial and stacked formations as shown in (Fig. 2).

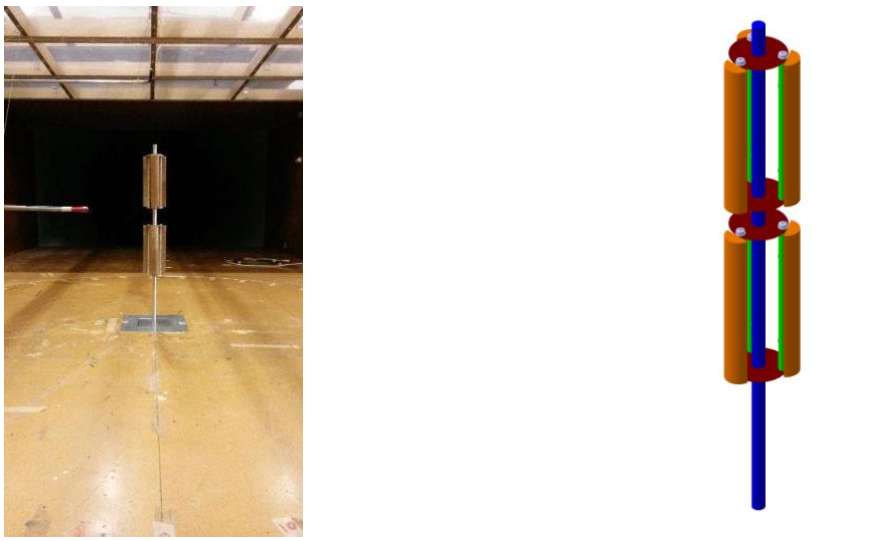

Fig. 1. Left Mast and 6 antennas wind tunnel, right Mast and 6 antennas CATIA V5 design

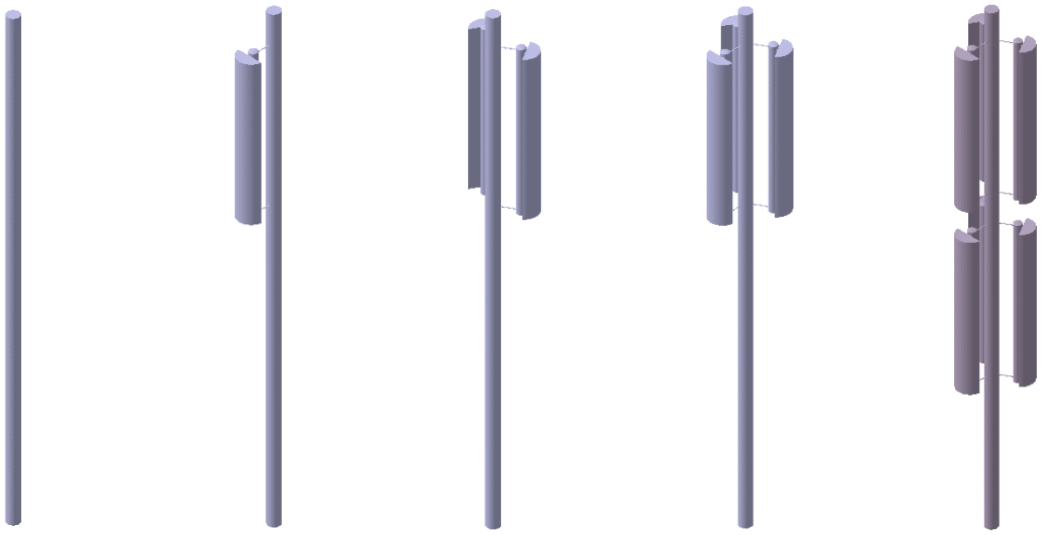

Fig. 2. CATIA V5 3D design, Mast only, Mast and 1 antenna, Mast and 2 antennas, Mast and 3 antennas, Mast and 6 antennas

Simulations were performed in ANSYS Fluent using the Reynolds-Averaged Navier-Stokes (RANS) method with the SST k-omega turbulence model. Several turbulence models were reviewed, with

RANS and SST k-omega models identified as the most effective for bluff body simulations such as telecommunication towers. These models are well-suited for external aerodynamic analysis of bluff bodies and allow for accurate prediction of separation and wake regions. To reduce RANS turbulence model uncertainty in outcomes prediction, a few measures were performed before each simulation in terms of geometry, fluid density, viscosity, grid, and boundary conditions [1].

The computational domain was defined following best practices, with domain extents based on mast height and antenna diameter using method of [2,3]. Five Body of Influence (BOI) regions were used to refine the mesh locally around critical geometry, including the antenna bodies and wake regions, according to [4] presented in (Fig. 3). The domain side view is shown in both (Fig. 4 and Fig. 5) and with all the necessary dimensions used. Boundary conditions included a uniform inlet velocity of 11.47 m/s and an outlet pressure set to atmospheric as per [5]. Air density and viscosity were matched to wind tunnel conditions (ρ = 1.04068 kg/m^3, μ = 2.034e-5 Pa·s). Probe lines were used in the solver to extract wind velocity.

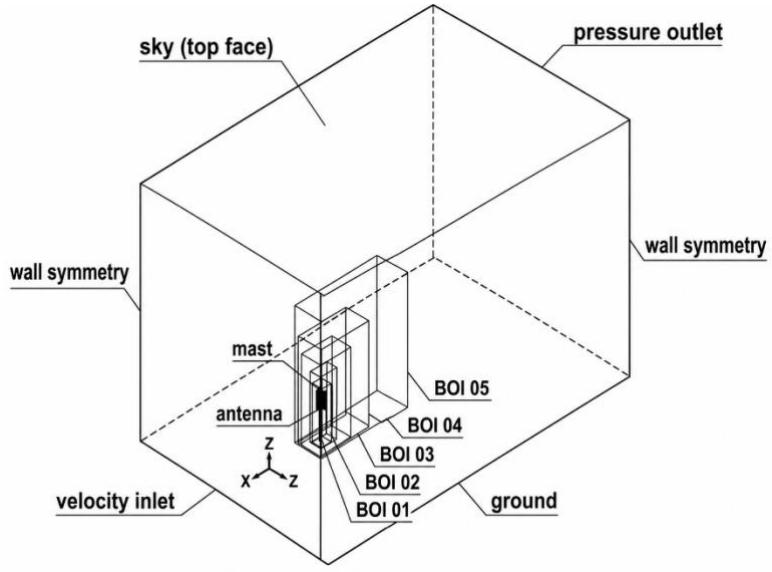

Fig. 3. CATIA V5 Domain Isometric View

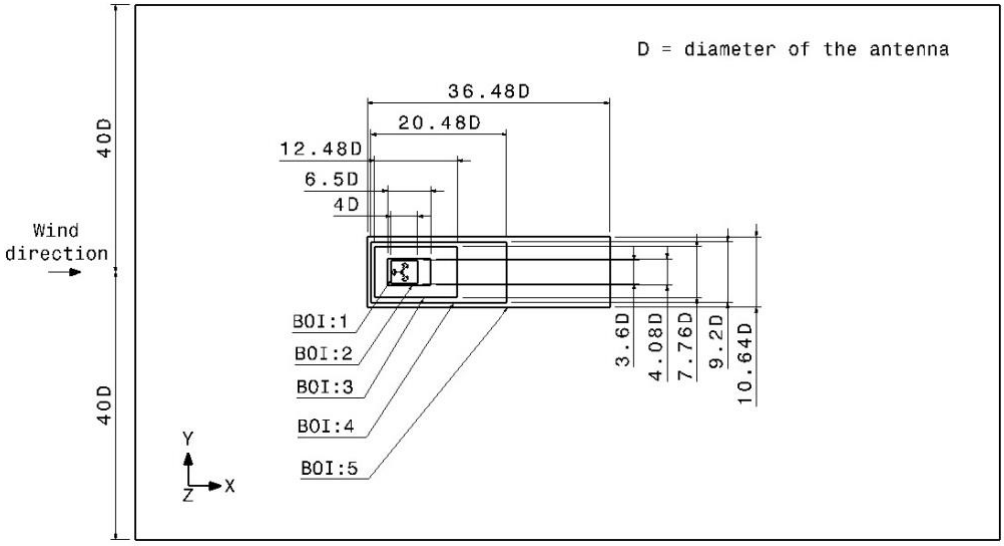

Fig. 4. CATIA V5 Domain Top View

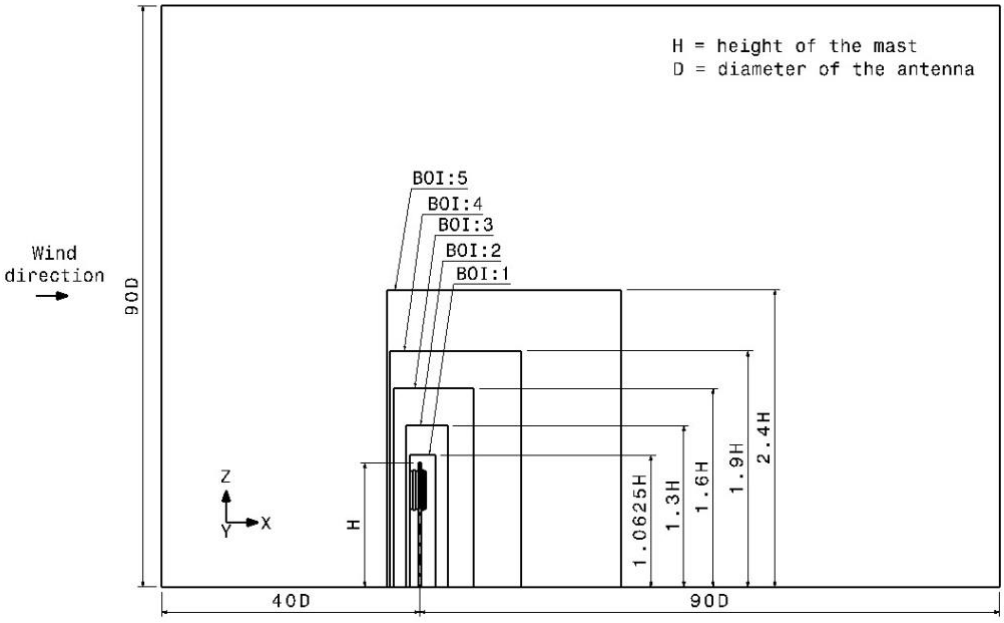

Fig. 5. CATIA V5 Domain Side View

2.1. Meshing Process in CFD

During the meshing process some guidelines from Qin were adapted in terms of meshing sizes, but each set of simulation in this study had unique sizes. With ANSYS® Fluent there are four types of mesh available in the watertight geometry interface, polyhexcore, hexcore, polyhedral and tetrahedral. Their availability is to do with different types of simulation that have to be done and adapted accordingly. If for example tetrahedral mesh type is used in the watertight geometry environment, once the geometry is transferred into solver interface there is an option to convert mesh to polyhedral [6]. In this study two types of mesh were adapted and used as suited, from polyhedral to tetrahedral (Fig. 6) illustrates the two types of mesh used in this study.

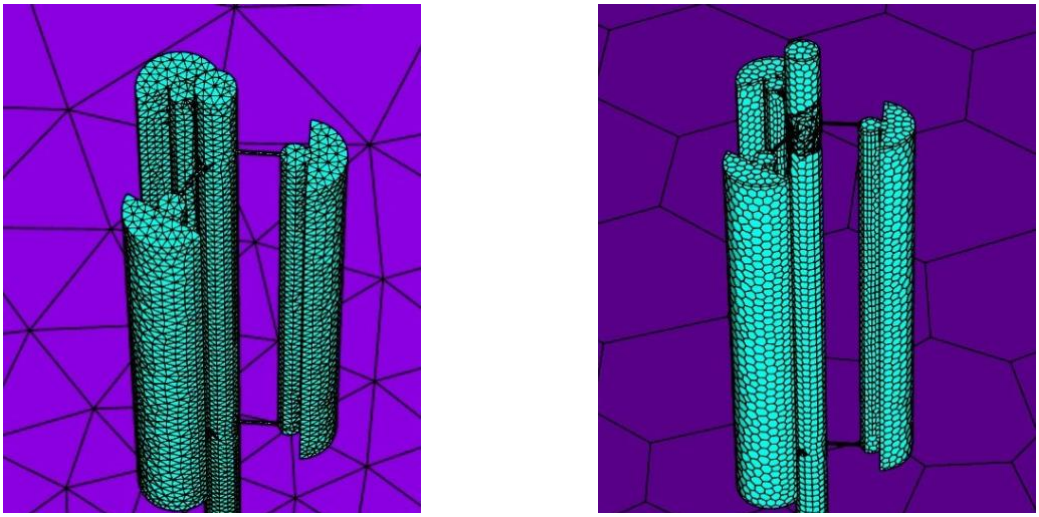

Fig. 6. Tetrahedral left and Polyhedral right mesh type mast with three antennas

Polyhedral meshes are generally associated with improved solver stability and reduced CPU time compared to tetrahedral meshes. Transitioning between mesh types within the solver is also efficient. Furthermore [7], emphasis more on the four types of mesh from watertight interface and in terms of mesh cells count, and preference. The combination of mesh type and inflation layers on the mast, either with or without antennas, varied throughout the experiment, although the domain or volume remained constant. This approach was necessary due to differences in geometry for each experiment. With the body of influence introduced (BOIs) enables localized mesh refinement in critical areas, such as the wake zone or antenna interfaces, while maintaining coarser meshes in

other areas of the domain. Standard near-wall treatment function correlation in Fluent Solver was adapted in this study, which is set as the default under SST k-omega models. Correlation: blends between analytical expressions for the viscous sublayer and the logarithmic region, allowing consistent accuracy regardless of mesh refinements described by [8].

2.2. Drag Force and Force Coefficient Settings in CFD

The settings to capture both the drag force and force coefficient in CFD were done for both axis in X and Y directions as standards practice. Once a set of simulations is completed, these two forces can be extracted using azimuth direction of 0° and 180° as shown in (Fig. 7) these two angles were adapted in this study.

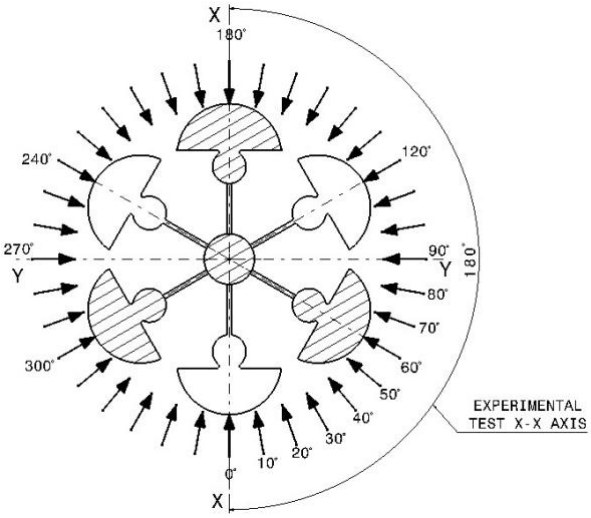

Fig. 7. Azimuth model set up in CFD domain

There is an advantage when using simulation software, especially in solver interface, a Notepad as a macro can easily be imported with coordinates and used to extract the required data. One aspect is referred to by several names; in a wind tunnel, it is known as the force coefficient, while in CFD settings, parameters, it is the drag coefficient and later becomes the pressure coefficient when the results are being processed in the solver. Mesh independence was verified through Grid Convergence Index (GCI) analysis over four mesh densities, with final simulations using polyhedral and tetrahedral mesh types ranging from 500k to 2.5 million cells, wind speed and dynamic pressure, and to determine force and moment coefficients. Table 1 displays the processed data from four simulations, prior to GCI.

Table 1. Results of four simulations, forces and force coefficients

Simulations	Iterations	Forces (N)	Force Coefficient	Mesh Elements Count
1	100	0.379	0.9980	265736
2	100	0.372	0.9424	528808
3	100	0.362	0.9168	1132456
4	100	0.356	0.9020	2466964

The GCI evaluation confirmed mesh independence, as the force values exhibited convergence requirements. The adaptation of the domain was based on consistent convergence behavior, force values, which aligned with physical wind tunnel results, and provided a robust foundation for subsequent analysis. The boundary layers on the mast were kept unchanged during these four simulation exercises. To account for the y plus value, the settings of boundary layers were taken as smooth layers, with the number of layers set at 20, transition ratio of 0.272, and with the growth rate of 1.2. Y+ value of the last set of completed simulations was extracted and was in the range of 0.0753 to 3.636 maximum.

The GCI was achieved using [9], method with 99.98 percent while using a polynomial line, an indication of good agreement during the experiment and continuation of using the same domain. Once the force and velocity pressure are extracted, it is easy to use the appropriate equations to find the force coefficient Table 2.

Table 2. Grid convergence study results for force and force coefficient

Performance parameter	Coarse	Medium	Fine						Asymptotic range 23-12
	f_3	f_2	f_1	$f_{h=0(12)}$	p	GCI_{12}	GCI_{23}	ε	
Force (N)	0.372	0.362	0.356	0.347	0.648	3.160	5.180	0.017	0.983
Force coefficient	0.9424	0.9168	0.902	0.8138	0.695	2.811	4.653	0.016	0.957
Mesh count	528808	1132456	2466964						

The extracted results were processed to verify the mesh converged solution by analyzing the variation of the drag force and drag coefficient in (Fig. 8) with increasing mesh densities. Parameters extracted from the solver solution, such as drag force, are both sensitive to mesh cell size and shape. The results are shown in (Fig. 9), in which the drag force stabilized beyond approximately 2.5 million elements, while the drag coefficient plateaued around 0.90.

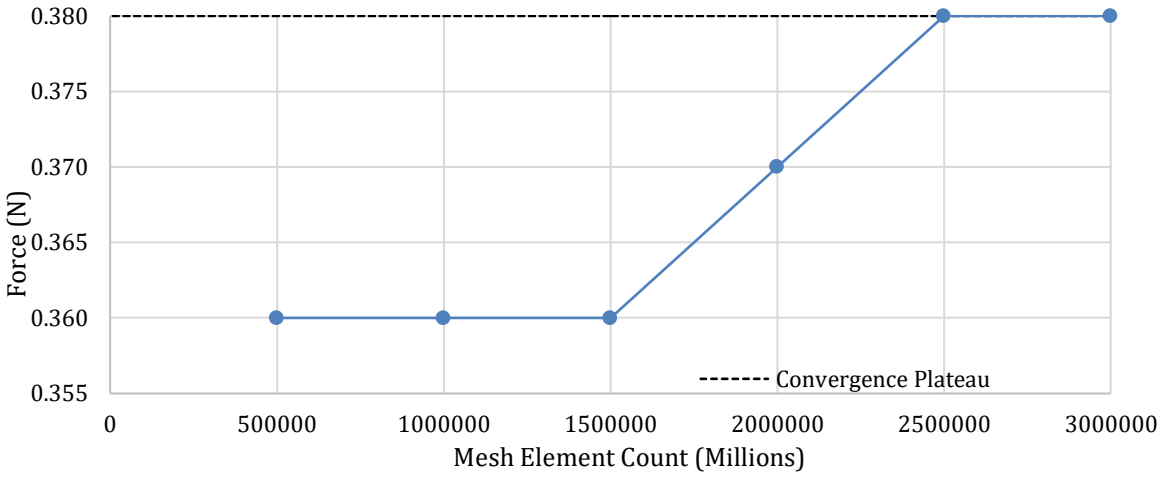

Fig. 8. Relationship between mesh element count and total drag force obtained from CFD

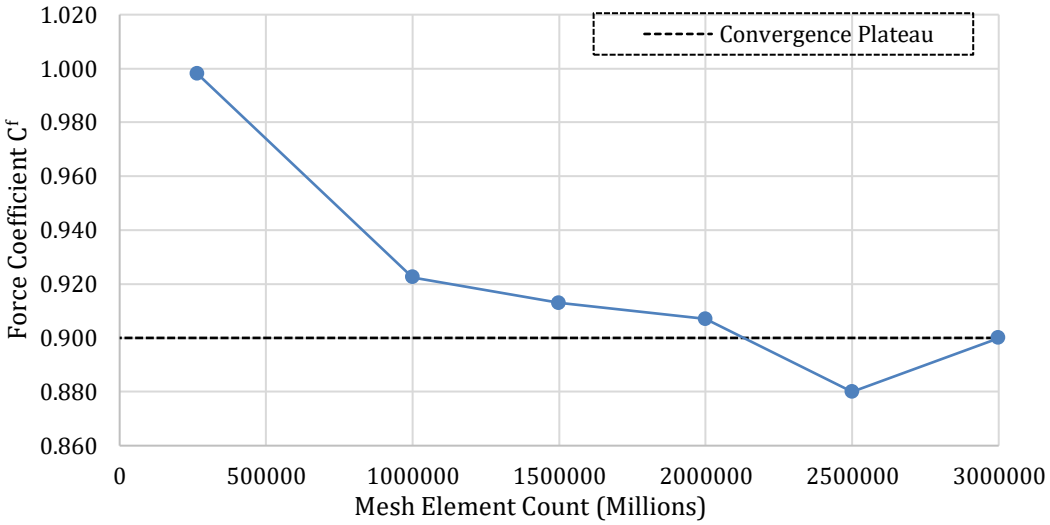

Fig. 9. Mesh element count versus drag coefficient C_d

Mesh convergence analysis confirmed that a mesh count above 2.5 million cells produced stable force and moment values, with minimal sensitivity to further refinement. Tetrahedral meshes resulted in nearly double the cell count compared to polyhedral meshes under equivalent refinement criteria. Results were compared with experimental data from CSIR wind tunnel conducted by Annandale.

3. Results

3.1. Parameters Extraction from Simulations Results

Once simulations have been completed in the CFD solver, all the elements like force, wind speeds, projected area, and velocity pressure were extracted from the solution file. Regarding the force coefficient, further steps were required that involved the use of Eqs (1), (2), (3), (4), and Eq (5) in a combination with standard codes and compared with wind tunnel.

- SANS 10255 (South Africa):

$$F = q_z \times A_{eff} \times C_g \times C_f \quad (1)$$

Where; F = resultant nominal wind force at height z (N), q_z = velocity pressure at height z (above atmospheric pressure) (N/m^2), A_{eff} = effective frontal area at height z (m^2), C_g = gust loading factor, C_f = force coefficient, z = height measured from the base to the centroid of the antenna (m)

- TIA-222-H (United States):

$$F = \frac{1}{2} \times \rho \times C_{dp} \times V^2 \times A \quad (2)$$

Where; F_w = wind force, ρ = air density, C_{dp} = profile drag coefficient, λ = length-to-width aspect ratio correction factor, V = wind velocity, A = cross-sectional area normal to wind direction

- EN 1993-3-1 and EN 1991-1-4 (Europe):

$$F_\omega = \frac{1}{2} \times \rho \times \left(C_f \times \Psi_r \times \Psi_\lambda\right) \times V^2 \times A \quad (3)$$

Where; F_w = wind load (N), C_{fo} = force coefficient for rectangular sections without rounded corners, Ψ_r = reduction factor for a rectangular section with rounded corners, Ψ_λ = end-effect factor, A = windward projected area (m^2), V = wind speed (m/s), ρ = air density (kg/m^3)

- AS 3995-1994 and AS/NZS 1170.2:2011 (Australia and New Zealand):

$$F = \left(\frac{1}{2} \times \rho_{air}\right) \times C_{fig} \times C_{dyn} \times \left(V_{des,\theta}\right)^2 \times A_z \quad (4)$$

Where; F = wind force (N), ρ_{air} = air density (kg/m^3), Vdes, θ = design wind speed in direction, C_{fig} = aerodynamic shape factor, C_{dyn} = dynamic response factor, A_z = reference area (m^2)

The refined equation used to isolate the antennas for the coefficient was:

$$C_{f,anenna} = \frac{F-(q_z \times A_{shaft} \times C_{f,shaft})}{q_z \times A_{antenna}} \quad (5)$$

Once all the data were processed, the comparison was conducted as the final phase. Table 3 represents the setup for the settings used for all four cases, including mesh sizes and the number of cells.

Time for simulations state: RANS Steady modelling was adopted, and Turbulence Mode: Viscous (SST k-omega) Menter adopted, wind speed 11.47 m/s, which remained static. The air density of 1.04068 kg/m^3 is derived from the wind tunnel data, whereas the viscosity of 0.00002034 is calculated through interpolation.

Probe lines as shown in (Fig. 10) were created and used in the solver to extract data results from the solver; their position did not change in all four simulation configurations. With probe lines using the function of line rake, to extract the wind pressure and wind speeds were extracted using the X-Y function in ANSYS solver.

Table 3. ANSYS Fluent parameter settings for Mast configurations

Parameters	Case 1	Case 2	Case 3	Case 4
	Mast with one antenna	Mast with two antennas	Mast with three antennas	Mast with two set of three antennas
Surface mesh size min	3.17383	3.17383	3.17383	3.17383
Surface mesh size max	100	81.22	200	125
Cell size max (mm)	100	103.5	262	100
Cell type	Tetrahedral	Polyhedral	Polyhedral	Polyhedral
Number of cells	371779	321263	313540	478120
Y+ range	0.055 to 16.6	0.072 to 61.179	0.187 to 352.233	0.060 to 90.713

CFD simulations produced results closely matching wind tunnel measurements. Deviations in wind speed and dynamic pressure were within 1%, while force coefficients differed by less than 6%. For the mast with three antennas, the calculated base bending moment from CFD was 0.18 Nm compared to 0.372 Nm from TIA-222-based calculations, indicating a 52% reduction due to shielding effects. Dynamic pressure was calculated using Eq (6) and used in conjunction with extracted force values to determine drag coefficients. Antenna-specific coefficients were derived by subtracting the mast-only contribution.

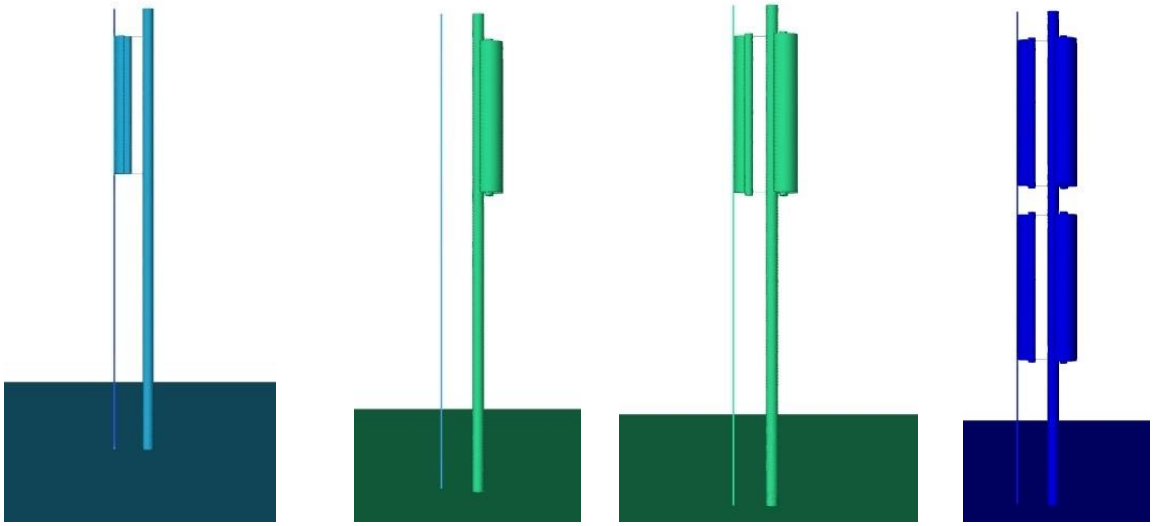

Fig. 10. Probe lines in the solver for Mast and different configurations

$$q_z = 0.5 \times \rho \times V^2 \tag{6}$$

3.2. Comparison of Standard Codes Force Coefficients

Using the standard codes from at least four regions, the force coefficients were processed while taking into consideration all their respective aspects and related equations. Each standard code has unique requirements that must be adhered to for the antenna force coefficient. The variation in the force coefficient of antennas results was easily noticeable due to the process of each standard code that had to be followed. In some of the cases results seem to be more conservative, when the number of antennas increases. The results from different standard codes were compared with those from wind tunnel results. The results from the wind tunnel, CFD, SANS 10255 and international codes: AS/NZS 1170.2, TIA-222, and EN 1991-1-4, of the cylinder without attachments, results are shown in (Fig. 11). Their variation is clear according to each code requirement, except for one that the Reynolds number must be accounted for EN 1991-1-4.

In (Fig. 12), are the force coefficients results for mast with antenna configurations from CFD, wind tunnel, and standard code. The difference in results for mast with one antenna is attributed due to standard codes elements aspect ratio assumptions, aero-dynamic shape factors, and wind exposure

classification. The variation for the force coefficient of the mast with two antennas attached differed in relation to the assumptions of elements highlighted, such as aspect ratio from TIA-222 and EN 1991-1-4, and the impact of aerodynamic factors from AS/NZS 1170.2, while the wind tunnel is still bound to SANS 10225, and CFD. For the mast three antennas attached, the force coefficient for both CFD and wind tunnel has shown a strong agreement. While for the standard code, variation still shows in the aspect ratio and shape factors. Looking at the force coefficients in of mast with six antennas configuration, there is agreement between wind tunnel and AS/NZS-1170.2, while there is a variation from CFD, TIA-222 and EN1991-1-4.

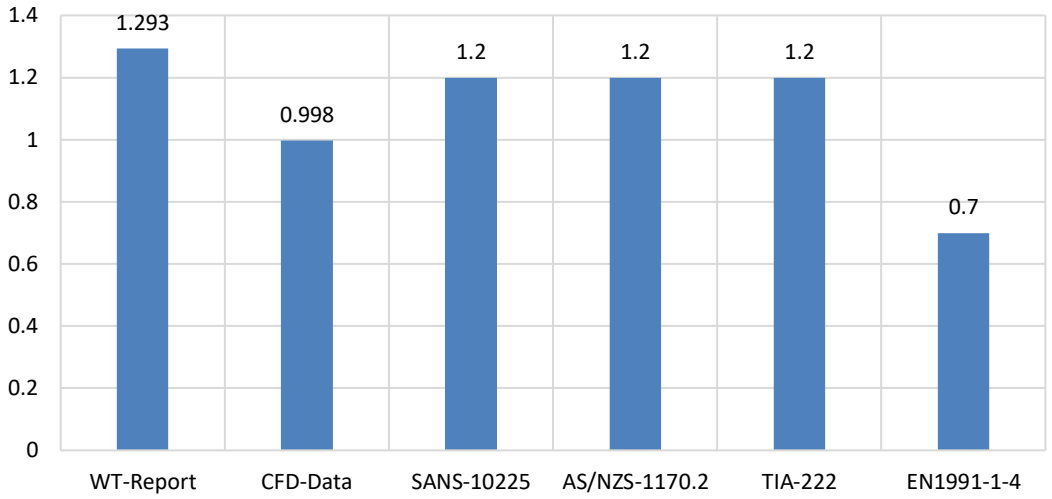

Fig. 11. Force coefficient for Mast only

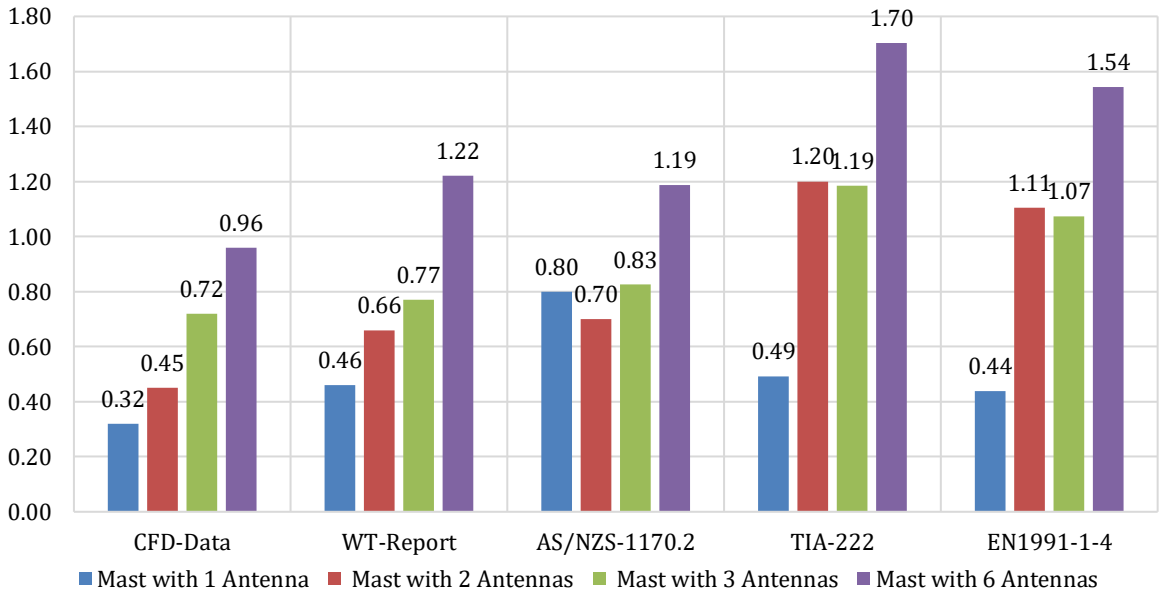

Fig. 12. CFD, wind tunnel and standard codes force coefficient for Mast with all configurations

3.3. CFD Force Coefficient for Mast with Three Antennas in Radial

ANSYS Fluent has several features that provide advantages which can be used up to a certain stage, as was the case in this study. The X, Y, and Z coordinates were generated in Excel, transferred to Notepad, and then imported into CFD solver to extract the force coefficients for statistical analysis at ten-degree intervals. The coordinates were generated following the principles and processes outlined by [10]. These were plotted using Excel, and the variances are visible at each 10-degree

interval. If desired, this process can be repeated at various heights of a telecommunication tower to obtain varied outcomes.

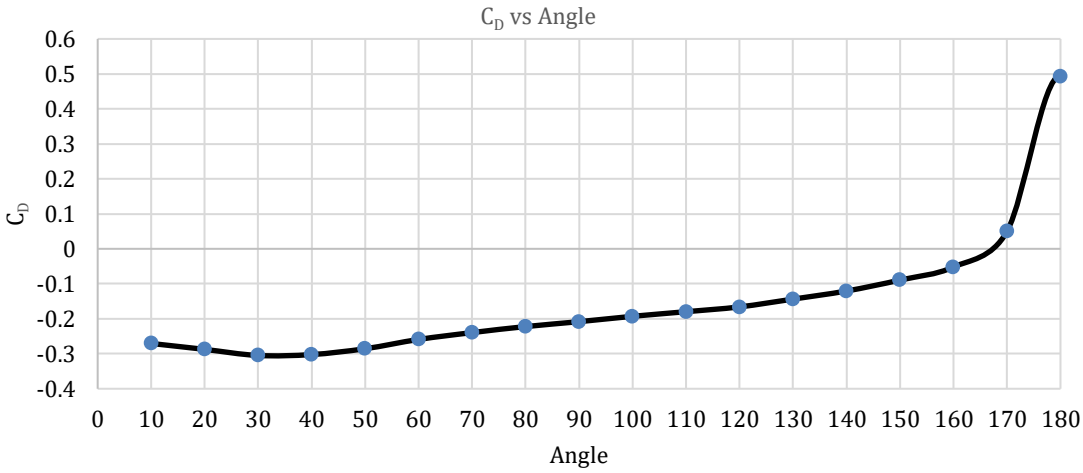

Fig. 13. CFD results for mast with one antenna; force coefficient at 10° intervals

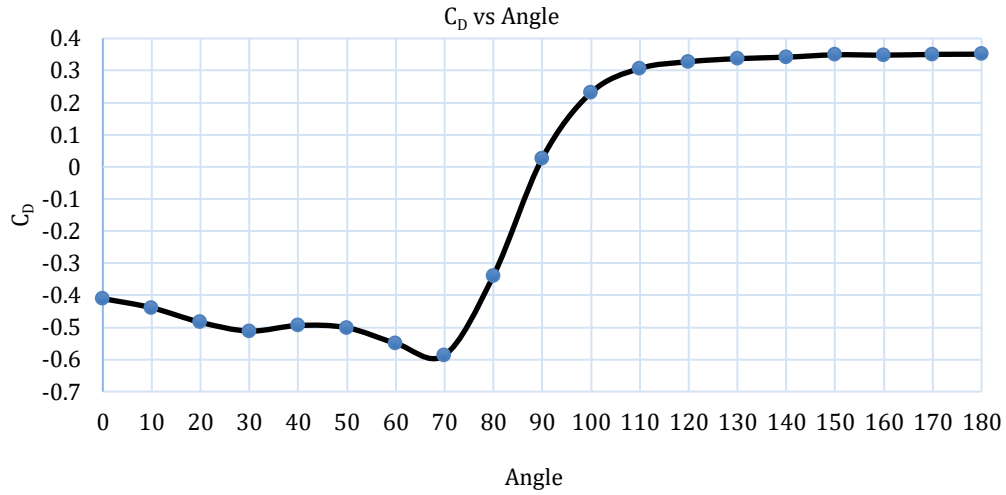

Fig. 14. CFD results for mast with two antennas; force coefficient at 10° intervals

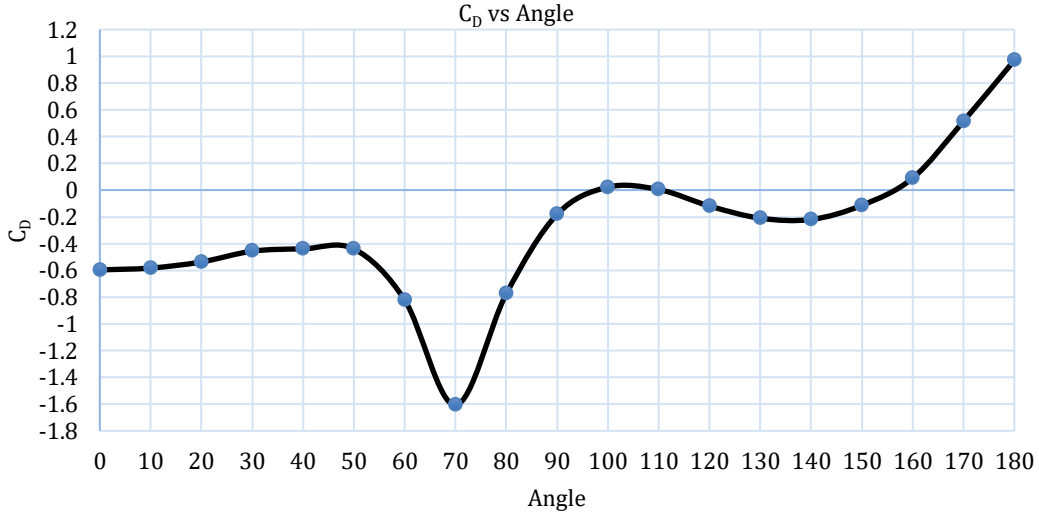

Fig. 15. CFD results for mast with three antennas; force coefficient measured at 10° intervals

This method resulted in an increased standard deviation in the force coefficient across the angles compared to previous setups, demonstrating that wind exposure for this arrangement is strongly orientation dependent. (Fig. 13) exhibits a unique fluctuation in force coefficient for a mast with a single antenna between 0° and 180°, representing the impact of geometrical profile. (Fig. 14) illustrate the force coefficient for a mast equipped with two antennas; the change in profile is unique due to the number of attachments. (Fig. 15) show this variance, with noticeable dips matching to the shielding position for mast with three antennas. (Fig. 16) demonstrate variation of force coefficient profile for the bottom profile, mast with six antennas showing a modest dip at 70 degrees when compared to the three attachments due to their height level positioning. In (Fig. 17), top force coefficient for the mast with six antennas this profile seems similar to the mast with three antennas in terms of shape.

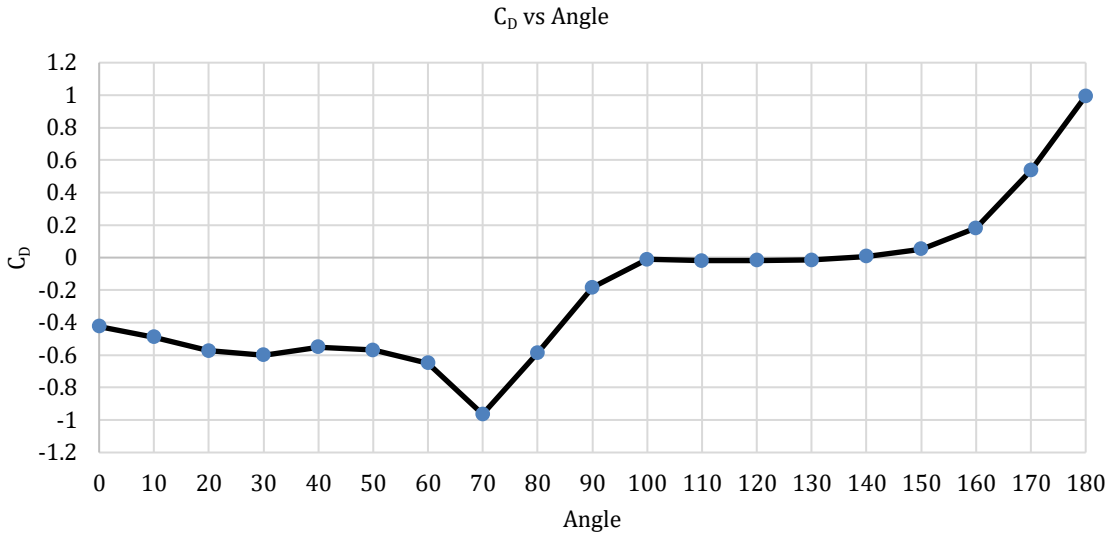

Fig. 16. CFD results for mast with six antennas; bottom force coefficient at 10° intervals

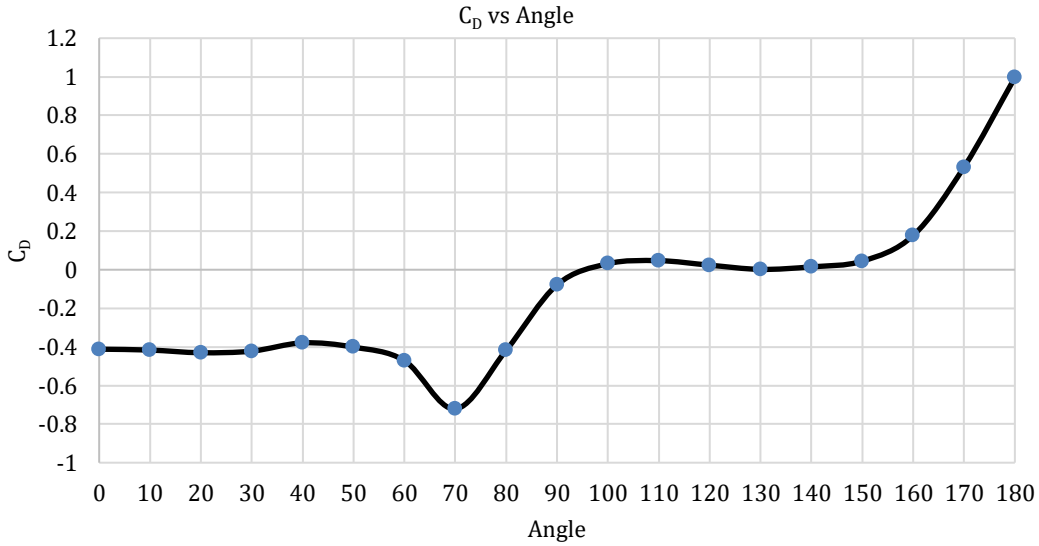

Fig. 17. CFD results for mast with six antennas; top force coefficient at 10° intervals

3.4. Bending Moments Comparison Between CFD and Design Code

The aim of this comparison was to evaluate the discrepancy between predicted bending moments from CFD and those obtained through conventional design code methods such as [11-16]. The procedure of design standards assumes that each antenna acts independently, contributing to full wind loads at a known height, whereas CFD accounts for aerodynamic shielding and interaction

effects. By quantifying this difference, the study tests the hypothesis that CFD can significantly reduce the design moment compared to traditional assumptions, particularly for the cluster antenna configurations as shown in Table 4. Table 5, represent the moment results for antenna configurations only.

Table 4. Moments for different mast configurations

System	Mast only (Nm)	Mast & 1 Antenna (Nm)	Mast & 2 Antennas (Nm)	Mast & 3 Antennas (Nm)	Mast & 6 Antennas (Nm)
WT	0.12	0.14	0.19	0.28	0.56
CFD	0.09	0.12	0.21	0.27	0.55

Table 5. Moments for antenna configurations

System	One Antenna (Nm)	Two Antennas (Nm)	Three Antennas (Nm)	Six Antennas (Nm)
WT	0.020	0.07	0.16	0.42
CFD	0.030	0.12	0.18	0.45

3.5. Governing equations for Design Code Wind Moments

Design codes typically estimate wind force on each attachment as using Eqs (1), (2), (3) and (4).

Where; $\rho = 1.04068$ kg/m^3 (air density), $C_d = 1.3$ (for Semi-Circular Cylinder, Convex Face Upstream), $A =$ frontal area of a single antenna (0.025 x 0.150 m^2), $V =$ wind speed from simulation, $F =$ wind force acting on one antenna

The bending moment at the base of the mast is:

$$M_{code} = \sum(F_i \times h_i) \tag{7}$$

For equal antenna heights:

$$M_{code} = N \times F \times h \tag{8}$$

Where; N: Number of antennas (1, 2, 3, or 6 depending on configuration), H: Height from mast base to the antenna center of pressure, this is the moment arm used in all calculations that follow.

3.6. Sample Calculation for Mast with Three Antennas

Each antenna set has:

$$A = 0.00375 \times 3 = 0.01125\ m^2 \tag{9}$$

Then;

$$F = \frac{1}{2} \times 1.04068 \times 1.3 \times 0.01125 \times (11.43)^2 \approx 0.992\ N \tag{10}$$

Then;

$$M_{code} = 1 \times 0.992 \times 0.375 = 0.372\ Nm \tag{11}$$

From Table 5 (CFD results) $M_{CFD} = 0.180\ Nm$

Reduction:

$$Reduction = \left(1 - \frac{0.180}{0.372}\right) \times 100 \approx 51.6\% \tag{12}$$

3.7. Summary of Moment Comparison

Table 6 and Figure 18 illustrate the percentage reduction in bending moments when using CFD simulations compared to traditional code-based computations in different antenna configurations. The reductions range from approximately 28% to 76%, highlighting the aerodynamic efficiency captured by CFD that is not considered in conventional design assumptions.

Table 6. Summary of moment comparison

Configuration	CFD Moment (Nm)	Code Moment (Nm)	Reduction (%)
One Antenna	0.030	0.125	76%
Two Antennas	0.120	0.249	52%
Three Antennas	0.180	0.372	52%
Two Sets of 3 Antennas	0.450	0.627	28%

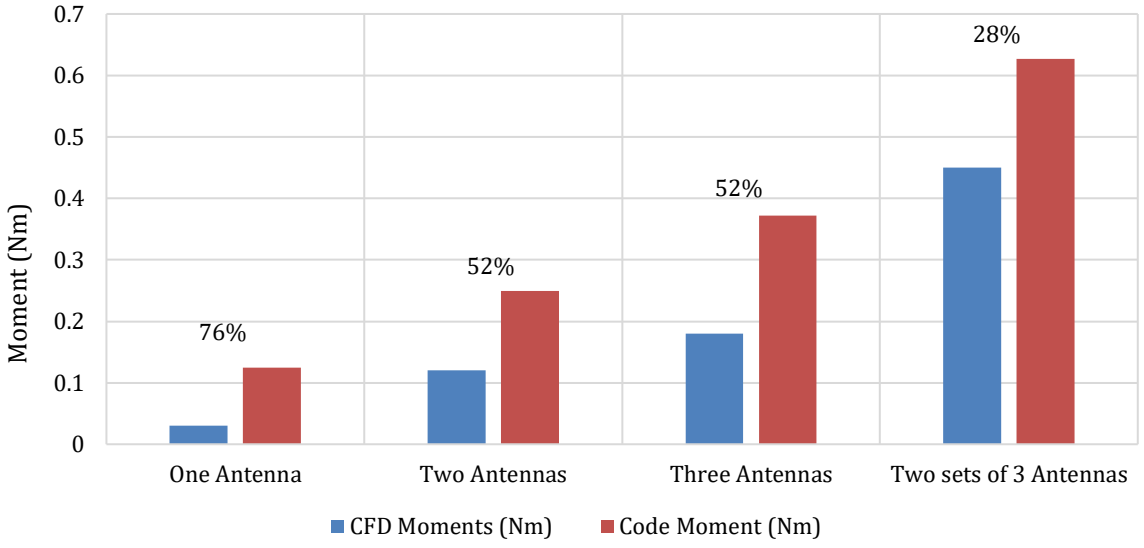

Table 7. Reduction in Bending Moments (CFD vs Code-Based) by Antenna Configuration

3.8. Projected and Effective Areas

Across all antenna configurations, the projected areas derived from CFD (via solver-based projection in either X or Y direction axis) and CAD (via geometric measurement) showed consistent alignment, with discrepancies typically under 5%. For example, the three-antenna configuration yielded CFD and CAD areas of 0.0062 m^2 and 0.0064 m^2, respectively. In the most complex setup with two tiers of three antennas, the solver and CAD returned 0.0089 m^2 and 0.0091 m^2, respectively.

4. Discussion

The results highlight the limitations of standard design codes in capturing aerodynamic interactions among multiple antennas. Design codes such as TIA-222, SANS 10225, and EN1991-1-4 treat antennas as fully exposed independent elements, ignoring aerodynamic shielding, which CFD captures effectively. In the six-antenna configuration, shielding led to a 28% reduction in predicted base moment.

Furthermore, projected and effective frontal areas derived from CFD matched within 5% of CAD-based measurements. This agreement confirms that CFD-based geometry projection is reliable for force coefficient computation. The ability to simulate full-scale geometries without scaling, combined with accurate turbulence modeling and refined meshing strategies, makes CFD a viable substitute for physical testing.

The integration of artificial intelligence in CFD is briefly discussed, noting its growing role in solver automation and predictive modeling by [17]. Although not directly applied in this study, the potential for AI-enhanced CFD to further reduce simulation time and increase accessibility is significant as discussed by [18-20].

An example of retrieved results following simulation for a mast and one antenna can be found in Appendix A.

- Scaled residuals
- Iterations vs Forces in X direction
- Iterations vs Forces in Y direction
- Velocity Magnitude
- Dynamic Pressure
- X-Y-Z Coordinates used to extract Force Coefficient

5. Conclusion and Recommendations

5.1 Conclusion

This study demonstrates the effectiveness of CFD in assessing wind loads on monopole telecommunication towers, for various antenna configurations. Key findings include:

- Mesh independence was achieved and validated using GCI methodology.
- ANSYS Fluent Academic Version 2023-R2 was available for simulations using, RANS SST k-omega turbulence modeling provides desired reliable results on standard laptop hardware.
- CFD findings were processed and compared to the wind tunnel report, taking into account the codes SANS-10255, AS/NZS-117.2, TIA-222, and EN1991-1-4. Five different designs configuration were tested: a bare mast with no attachments, a mast with one antenna, two antennas, a three-antenna radial layout, and a two-tiered arrangement with six antennas. Variations in the force coefficient comparison were obvious, owing to certain of the aspect criteria of each code.
- When compared to the wind tunnel, force coefficients could be derived at various heights of antenna designs using Notepad as a macro and processed in less amount of time, proving the advantage of CFD.
- CFD can reduce design code bending moment of estimates by up to 52% due to aerodynamic shielding effects between clustered antennas.
- CFD force coefficients aligned within 6% of wind tunnel results, validating simulation accuracy.
- The deviation in force coefficients between CFD and physical tests remained below 5.5% across all configurations, reinforcing confidence in the numerical approach.
- Projected areas from solver output agree closely with CAD measurements, ensuring accurate force predictions.
- The adoption of CFD enables more accurate, less conservative, and economically efficient structural assessments of monopole towers. Further it advocates for the integration of CFD into standard engineering practice, potentially in combination with AI tools for further optimization.
- Rapid and accurate examination of the structural integrity of existing telecommunications towers could also lead to the recommissioning of underutilized infrastructure. Furthermore, the implementation of CFD simulations during the design and site selection phases for new towers could enhance predictive capabilities, enabling registered professionals to anticipate environmental impacts and structural performance with greater precision before or during construction.
- Thus, the findings in this study have the potential to contribute meaningfully to the optimization and sustainability of telecommunications infrastructure. The design of telecommunication towers and antenna configurations could be optimized, analysis by registered professional can go in much deeper detail; giving a broader option when

designing. Important elements such as, forces, wind speed, moments, dynamic pressure and force coefficient were successfully comparing to the wind tunnel data during this study.

5.2 Recommendations

Even though this study has shown how useful CFD is for designing telecommunication towers, there are still a number of areas that could be used in more studies:

- Inclusion of Dynamic Wind Effects: Steady-state wind simulations were the main focus of this study. Future study should use transient simulations to capture time-dependent phenomena, including vortex-induced vibration (VIV), galloping, and aeroelastic flutter, in order to further the understanding of fatigue behavior over time.
- Expansion to Full-Scale Structures: Although the simulations were scaled to match the wind tunnel models, full-scale simulations are recommended. This would necessitate high-speed computing resources but would yield insights into real-world aerodynamic performance at operating heights.
- Incorporation of Terrain and Environmental Effects: Realistic environmental factors, such as terrain roughness, atmospheric boundary layer profiles, and thermal gradients, should be included in the CFD model to simulate more accurate wind flow patterns.
- Experimental Validation with Full-Scale Instrumentation: In-situ measurements of actual towers under wind loading would offer further validation of CFD predictions. Sensor arrays mounted on towers could provide real-time force and displacement data for benchmarking.
- Development of Simplified CFD-Based Design Guidelines: The objective is to develop efficient, semi-automated CFD workflows and simplified adjustment factors that may be integrated into normal design practices, thereby connecting advanced simulations with routine engineering applications.
- Exploration of AI-Augmented CFD: With recent advances in artificial intelligence, future studies could investigate the use of AI to accelerate mesh generation, predict force coefficients, forces, or optimize tower geometries in real-time during simulation.
- Evaluation of Additional Attachment Types: The study focuses on cylindrical and planar antennas. Further study should evaluate the aerodynamic behavior of a broader range of attachments, including parabolic dishes, Remote Radio Units (RRU), and camouflaged (e.g., artificial tree-type) structures.

By pursuing these directions, future study can enhance the accuracy, applicability, and efficiency of CFD in structural engineering field. Such efforts will contribute toward modernizing design practices, reduce excessive conservatism, and ensure safer, more economical infrastructure across the telecommunications industry.

Acknowledgement

The authors would like to thank the Department of Civil Engineering, Faculty of Engineering and the Built Environment, Tshwane University of Technology, for their dedication to providing both the laptop and access to the ASNYS Fluent Academic Version used for this study.

References

[1] Menter F, Lechner R. Best practice: RANS turbulence modeling in Ansys CFD, NTS, St. 320 Petersburg, Russia: ANSYS Germany, 2023.
[2] Qin P, Zhou Z. Aerodynamic analysis of the top structure of a monopole telecommunication tower: Impact of wind directions and diameters of the hexadecagonal tube body. Journal of Wind Engineering and Industrial Aerodynamics, 2022; 224, p.104946. https://doi.org/10.1016/j.jweia.2022.104946
[3] Franke J, Hellsten A, Schlunzen KH, Carissimo B. The COST 732 Best Practice Guideline for CFD simulation of flows in the urban environment: a summary. International Journal of Environment and Pollution, 2011; 44(1-4), pp.419-427. https://doi.org/10.1504/IJEP.2011.038443
[4] ANSYS®. How to set up box local refinement regions - add local sizing - Ansys fluent 305 watertight, 2024; https://www.youtube.com/watch?v=7g0N-0LTqXg
[5] Annandale H. Wind-Tunnel Testing of a Group of Three Evenly Spaced Antennae Mounted on a Monopole Steel Mast. Master's Dissertation, Pretoria: The Tshwane University of Technology. 2016.

[6] ANSYS®. How to add local sizing in Ansys fluent meshing - lesson 1, part-1 Accessed: 2023-10-20. https://www.youtube.com/watch?v=FElQIvgDmLc
[7] Mendis H. Better meshing using ANSYS fluent meshing. Accessed: 2024-08-01. https://www.linkedin.com/pulse/better-meshing-using-ansys-fluent.
[8] Fluent 2025 R1. Fluent Theory Guide, 2025 https://ansyshelp.ansys.com/public/account/secured?returnurl=//Views/Secured/corp/v251/en/flu_th/flu_th.html
[9] Roache PJ. Verification and validation in computational science and engineering (Vol. 895, p. 895). Albuquerque, NM: Hermosa, 1998.
[10] CFD_Mechanic, 2023. Plotting coefficient of pressure along circular cylinder at Re = 150. ANSYS CFD tutorials and courses. https://www.youtube.com/watch?v=PEJaDXUoPhY
[11] TIA-222-H, 2005. Structural Standard for Antenna Supporting Structures and Antennas. USA: 329 Telecommunications Industry Association.
[12] SABS. SANS 10225. South African National Standards: the design and construction of 327 lighting masts. Pretoria: SABS Standards Division, 2012.
[13] EN1993-3-1. Eurocode 3: Design of steel structures - Part 3-1: Towers, masts and 314 chimneys - Towers and masts. Europe: Eurocode, 2006.
[14] EN1991-1-4. Eurocode 1: Actions on structures - Part 1-4: General actions Wind actions. Europe: Eurocode, 2005.
[15] AS 3995. Design of steel lattice towers and masts. Australia: Australian Standard, 1994.
[16] AS/NZS. 1170.2. Structural design actions-Part 2: Wind actions. Australia: 308 Australian/New Zealand Standard, 2016.
[17] Yuan S, Ajam H, Sinnah ZAB, Altalbawy FM, Ameer SAA, Husain A, Al Mashhadani ZI, Alkhayyat A, Alsalamy A, Zubaid RA, Cao Y. The roles of artificial intelligence techniques for increasing the prediction performance of important parameters and their optimization in membrane processes: A systematic review. Ecotoxicology and Environmental Safety. 2023; 260, p.115066. https://doi.org/10.1016/j.ecoenv.2023.115066
[18] Ao Y, Li Y, Gong J, Li S. An artificial intelligence-aided design (AIAD) of ship hull structures. Journal of Ocean Engineering and Science, 2023; 8(1), pp.15-32. https://doi.org/10.1016/j.joes.2021.11.003
[19] Li L, Lange CF, Ma Y. Artificial intelligence aided CFD analysis regime validation and selection in feature-based cyclic CAD/CFD interaction process. Computer-Aided Design and Applications, 2018; 15(5), pp.643-652. https://doi.org/10.1080/16864360.2018.1441230
[20] Williams Z, Moiz A, Cung K, Smith M, Briggs T, Bitsis C, Miwa J. Generation of Rate-of-Injection (ROI) profile for Computational Fluid Dynamics (CFD) model of Internal Combustion Engine (ICE) using machine learning. Energy and AI, 2022; 8, p.100148. https://doi.org/10.1016/j.egyai.2022.100148

Appendix

A. Extracted CFD simulation data for the mast and one Antenna

A.1. Solution Monitors Scaled Residuals

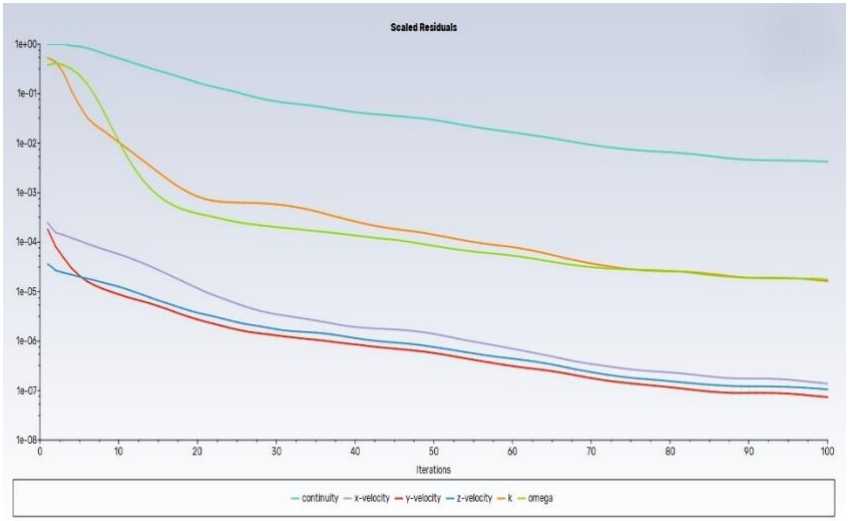

Fig. A. 1. Solution monitor scaled residuals

A.2. X-Direction Force vs Iterations

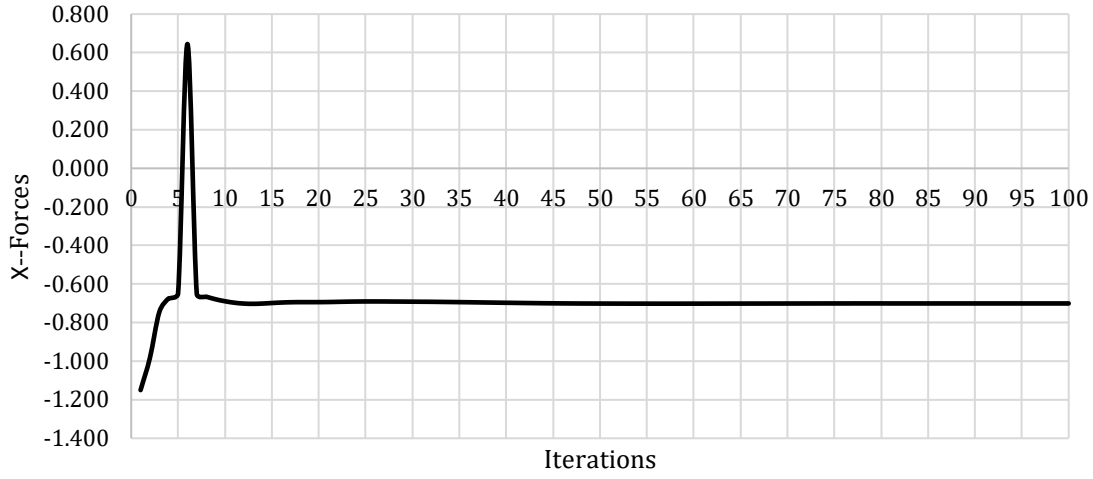

Fig. A. 2. X-Force vs Iterations

A.3. Y-Direction Force Iterations

Fig. A. 3. Y-Force vs Iterations

A.4. Velocity Magnitude

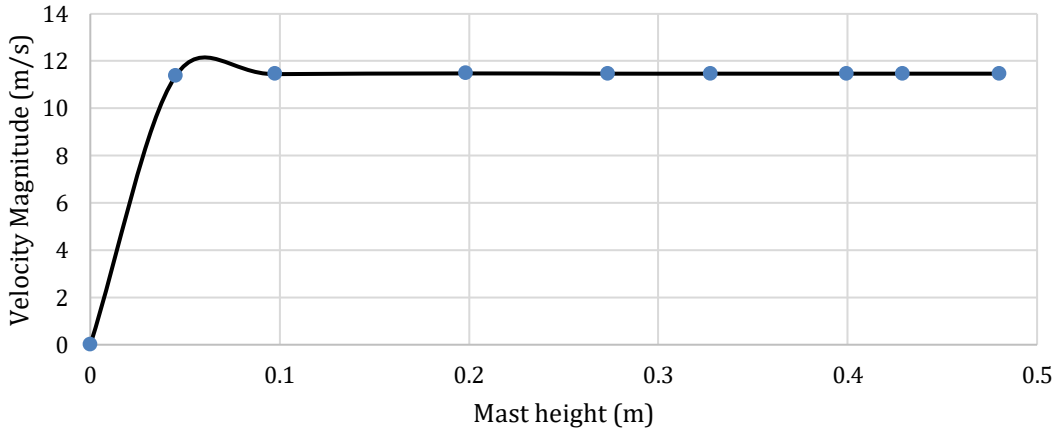

Fig. A. 4. Velocity magnitude vs Mast height

A.5. Dynamic Pressure

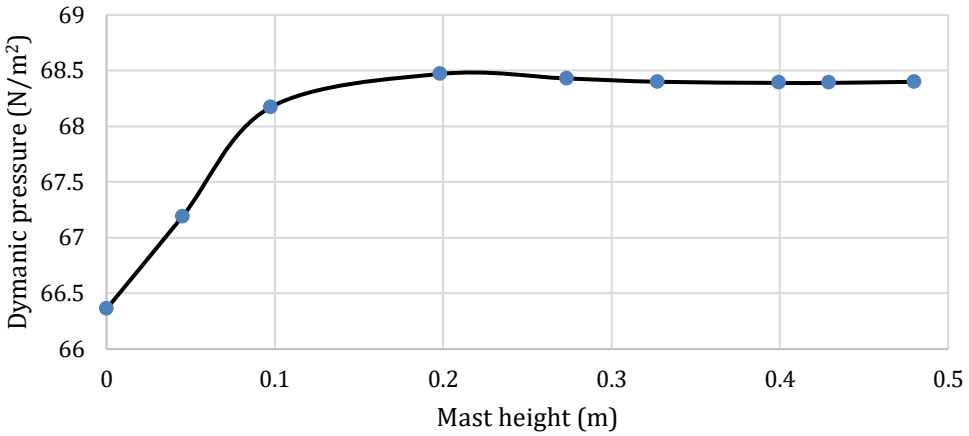

Fig. A. 5. Dymanic pressure vs Mast height

A.6. Notepad X-Y-Z Coordinates

Table A. 1. Coordinates points X-Y-Z

Points	Angle	X (m)	Y (m)	Z (m)
surface/point-surface ptname0	0°	0,037	0	0,375
surface/point-surface ptname1	10°	0,036438	0,006425	0,375
surface/point-surface ptname2	20°	0,034769	0,012655	0,375
surface/point-surface ptname3	30°	0,032043	0,0185	0,375
surface/point-surface ptname4	40°	0,028344	0,023783	0,375
surface/point-surface ptname5	50°	0,023783	0,028344	0,375
surface/point-surface ptname6	60°	0,0185	0,032043	0,375
surface/point-surface ptname7	70°	0,012655	0,034769	0,375
surface/point-surface ptname8	80°	0,006425	0,036438	0,375
surface/point-surface ptname9	90°	0	0,037	0,375
surface/point-surface ptname10	100°	-0,00643	0,036438	0,375
surface/point-surface ptname11	110°	-0,01266	0,034769	0,375
surface/point-surface ptname12	120°	-0,0185	0,032043	0,375
surface/point-surface ptname13	130°	-0,02378	0,028344	0,375
surface/point-surface ptname14	140	-0,02834	0,023783	0,375
surface/point-surface ptname15	150°	-0,03204	0,0185	0,375
surface/point-surface ptname16	160°	-0,03477	0,012655	0,375
surface/point-surface ptname17	170°	-0,03644	0,006425	0,375
surface/point-surface ptname18	180°	-0,037	0	0,375